Structure and Dynamics of Helix-0 of the N-BAR Domain in Lipid Micelles and Bilayers

Christian Löw,* Ulrich Weininger,* Hwankyu Lee,† Kristian Schweimer,‡ Ines Neundorf,§ Annette G. Beck-Sickinger,§ Richard W. Pastor,‡ and Jochen Balbach*¶

*Institut für Physik, Biophysik, Martin-Luther-Universität Halle-Wittenberg, D-06120 Halle (Saale), Germany; †Laboratory of Computational Biology, National Heart, Lung, and Blood Institute, National Institutes of Health, Bethesda, MD 20892; ‡Lehrstuhl Biopolymere, Universität Bayreuth, 95447 Bayreuth, Germany; §Institut für Biochemie, Fakultät für Biowissenschaften, Pharmazie und Psychologie, Universität Leipzig, D-04103 Leipzig, Germany; and ¶Mitteldeutsches Zentrum für Struktur und Dynamik der Proteine (MZP), Martin-Luther-Universität Halle-Wittenberg, Germany

ABSTRACT Bin/Amphiphysin/Rvs-homology (BAR) domains generate and sense membrane curvature by binding the negatively charged membrane to their positively charged concave surfaces. N-BAR domains contain an N-terminal extension (helix-0) predicted to form an amphipathic helix upon membrane binding. We determined the NMR structure and nano-to-picosecond dynamics of helix-0 of the human Bin1/Amphiphysin II BAR domain in sodium dodecyl sulfate and dodecylphosphocholine micelles. Molecular dynamics simulations of this 34-amino acid peptide revealed electrostatic and hydrophobic interactions with the detergent molecules that induce helical structure formation from residues 8–10 toward the C-terminus. The orientation in the micelles was experimentally confirmed by backbone amide proton exchange. The simulation and the experiment indicated that the N-terminal region is disordered, and the peptide curves to adopted the micelle shape. Deletion of helix-0 reduced tubulation of liposomes by the BAR domain, whereas the helix-0 peptide itself was fusogenic. These findings support models for membrane curving by BAR domains in which helix-0 increases the binding affinity to the membrane and enhances curvature generation.

INTRODUCTION

Proteins play fundamental roles in modulating the structure of lipid bilayers. Processes such as membrane fusion, budding, or tubulation are associated with changes in membrane curvature. The banana-shaped BAR domains have been identified throughout eukarya as regulators of membrane remodeling processes. They sense and curve membranes, and participate in numerous cytoskeletal and nuclear processes, such as clathrin–mediated endocytosis or organization of the T-tubule network in the muscle (1–10). Point mutations in the BAR domain of Bin1 found in patients with centronuclear myopathy cause a dysfunction of the latter process (11).

The crystal structures of the human and *Drosophila* amphiphysin BAR domain (12,13) reveal a crescent-shaped homodimer with a positively charged concave surface. This finding suggests that driving and/or sensing curvatures of membranes by BAR domains occurs by binding of negatively charged membranes to this positively charged surface (13). Some BAR domains (denoted N-BAR) contain an N-terminal extension with an amphipathic character that is predicted to undergo a random coil to helix transition by binding to the membrane (13). This extension, termed helix-0, shows no electron density in the crystal structure (14). In vitro, BAR domains can induce curvature in liposomes, which results in narrow tubes (tubulation) (15). Recent experimental and theoretical studies (16) with N-BAR domains indicate that helix-0 embeds in the lipid bilayer and strongly increases the ability to tubulate liposomes. The insertion of amphipathic helices into hydrophobic phases of the bilayer has been proposed to be a general mechanism for curvature generation during vesicle budding as shown in amphiphysin (13) and other examples (17–19). Experimental evidence for structure induction and insertion of the amphipathic helix has been derived from circular dichroism (CD) and electron paramagnetic resonance spectroscopy (EPR) (13,14,20,21). There are currently three candidate curvature-generating mechanisms: 1), the local spontaneous curvature; 2), the bilayer coupling; and 3), the scaffolding (22). The scaffold mechanism assumes that the intrinsic curvature of the BAR domain forces the membrane shape, as opposed to a deformation of the lipid bilayer by a shallow (spontaneous curving) or deep (bilayer-coupling) insertion of an amphipathic helix.

To obtain further insights into the predicted N-terminal amphipathic helix of N-BAR domains, we studied helix-0 of the human Bin1/Amphiphysin II BAR domain (N-BAR) in detergent and lipid environments by high-resolution NMR spectroscopy and molecular dynamics (MD) simulations. Structure calculation, dynamic measurements, and a fast amide proton exchange confirmed the earlier proposed amphipathic character of the induced helix but also revealed a disordered N-terminal part of the amphipathic helix that is highly flexible

Submitted March 28, 2008, and accepted for publication July 3, 2008.

Address reprint requests to Jochen Balbach Institut für Physik, Fachgruppe Biophysik, Martin-Luther-Universität, Halle-Wittenberg, D-06120 Halle (Saale), Germany. Tel.: 49-345-55-28550; Fax: 49-345-55-27161; E-mail: jochen.balbach@physik.uni-halle.de.

Abbreviations: BAR, bin/amphiphysin/rvs-homology; DPC, dodecylphosphocholine; EM, electron microscopy; 2D, two-dimensional; 3D, three-dimensional; FRET, fluorescence resonance energy transfer; MEXICO, measurements of exchange rates in isotopically labeled compounds; OG, n-Octyl-β-D-glucopyranoside; SDS, sodium dodecyl sulfate.

Editor: Arthur G. Palmer 3rd.

0006-3495/08/11/4315/09 $2.00

doi: 10.1529/biophysj.108.134155

and exposed to the solvent. We also considered the balance of electrostatic and hydrophobic interactions. Last, a tubulation assay of liposomes analyzed by EM or FRET showed that the isolated N-BAR peptide was fusogenic.

MATERIALS AND METHODS

Expression and purification of the N-BAR and BAR domain and the N-BAR peptide of human Bin1/Amphiphysin II

The plasmid of the BAR domain of human Bin1/Amphiphysin II was a kind gift of E. D. Laue (Cambridge). The histidine-tagged recombinant protein was expressed in *E. coli* BL21(DE3) and purified as described previously (12). The N-BAR peptides were expressed as a SUMO fusion protein and cleaved by the SUMO protease (23) or synthesized by solid-phase peptide synthesis. Further details are provided in the Supplementary Material, Data S1.

Liposomes and tubulation assay

Small unilamellar vesicles were prepared from total bovine brain lipids (Folch fraction 1; Sigma B1502; Sigma-Aldrich, Munich, Germany) in 20 mM Hepes, 150 mM NaCl, pH 7.4, by extrusion (pore size of 100 nm) using a Liposofast extruder (Avestin, Ottawa, Ontario, Canada) as described previously (13). For tubulation assays, N-BAR domain and different constructs (5 μM for N-BAR and BAR, 10 μM for N-BAR peptides) were mixed with brain lipid liposomes (0.2 mg/ml) for 30 min at room temperature and then processed for negative staining. For EM analysis, carbonized copper grids (Plano, Wetzlar, Germany) were pretreated for 1 min with bacitracin (0.1 mg/ml). After air-drying, protein lipid mixture diluted 5-fold with 20 mM Hepes, 150 mM NaCl, pH 7.4, was applied for 3 min. Subsequently, grids were again air-dried. Samples were negatively stained with 1% (w/v) uranyl-acetate and visualized in an electron microscope (Zeiss EM 900; Carl Zeiss GmbH, Jena, Germany) operating at 80 kV.

FRET assay of membrane fusion

Membrane fusion was measured by FRET using an FP-6500 spectrofluorometer (Jasco, Groß-Umstadt, Germany). Two populations of liposomes composed of bovine brain lipids, one unlabeled and one labeled with 2% each of *n*-[7-nitro-2-1,3-benzoxadiazole-4-yl]-egg-phosphatidylethanolamine and *n*-[lissamine rhodamine B]-egg-phosphatidylethanolamine, were mixed at a 9:1 unlabeled/labeled ratio and 0.25 mg/ml total lipid in 20 mM Hepes, 150 mM NaCl, pH 7.4, at 25°C in the presence of different concentrations of N-BAR and various constructs (concentration range: 1–15 μM for N-BAR and BAR, 5–50 μM for N-BAR peptide constructs). The excitation wavelength was 450 nm, and the emission spectrum was recorded from 480 to 700 nm after several time points. To obtain a value for donor fluorescence, 1% Triton X-100 was added. Kinetics of membrane fusion was followed by fluorescence increase of the donor fluorescence at 530 nm after excitation at 450 nm.

CD

Far-ultraviolet (UV) CD spectra of BAR domain and mutants were measured in the presence and absence of Folch liposomes in 20 mM Hepes, 150 mM NaCl, pH 7.4, at 15°C with a J815A spectropolarimeter (Jasco). 10 μM protein was incubated with 0.2 mg/ml Folch liposomes and degassed for 5 min before measurement. The N-terminal peptide was measured in the presence of different detergents (SDS, OG, DPC) and Folch liposomes. The signals from pure liposomes or micelles were subtracted from the sample spectra as blanks.

Sample preparation for NMR

N-BAR peptide was dissolved in 20 mM sodium phosphate, pH 7.4 (90% H_2O/10% ^2H_2O) containing either d_{38}-DPC or d_{25}-SDS micelles and 0.03% NaN_3. The final ^{15}N-labeled N-BAR peptide samples contained 1 mM protein and 200 mM d_{38}-DPC or 150 mM d_{25}-SDS. A 1 mM ^{15}N-labeled N-BAR peptide sample without detergent was prepared as a reference.

NMR spectroscopy

NMR spectra were acquired with a Bruker Avance 800, Bruker Avance 700 equipped with a cryoprobe, and a Bruker Avance II 600 spectrometer (all obtained from Bruker BioSpin, Rheinstetten, Germany) in 20 mM sodium phosphate buffer, pH 7.4, containing 10% ^2H_2O at 25°C; the free N-BAR peptide experiments, however, were carried out at 15°C and the extended N-BAR peptide (1–44 residues) at pH 6.0 and at 15°C. The N-BAR peptide in SDS and DPC micelles and the unbound form were assigned by 3D-^{15}N TOCSY-HSQC and 3D-^{15}N-NOESY-HSQC (complete assignments were deposited in the Biological Magnetic Resonance Bank database). For structure calculation of SDS- and DPC-bound N-BAR peptide, an additional 2D NOESY spectrum was recorded and a 3D HNHA spectrum was recorded for the SDS-bound form. For further investigations, a ^{15}N heteronuclear nuclear Overhauser enhancement (NOE) and a MEXICO proton-exchange experiment (24) were performed. The ordinate in Fig. 5 corresponds to the NMR crosspeak intensity at the respective exchange time divided by intensity in a reference experiment. Spectra were processed with NMRpipe (25) and analyzed with NMRView (26).

Structure calculation

Distance restraints were obtained from 3D ^{15}N-NOESY-HSQC and 2D NOESY and used as ambiguous constraints for structure calculation with ARIA (27). Backbone dihedral restraints were calculated from chemical shifts using TALOS (28). It should be noted that the random coil values of TALOS are not optimized for the micellar environment. ARIA runs with and without TALOS restraints, however, gave the same overall topology and curvature, but root mean-square deviation values were reduced with these restraints and therefore TALOS was included in the final run. Structure geometry was analyzed with PROCHECK (29). The preceding structure calculations did not rely on any of the MD results.

Computational methods

In principle, the peptide micelle complex could be assembled from a solution of dispersed lipids and an unfolded peptide. However, self-assembly of SDS micelles from 70 to 100 monomers in ~10000 waters was incomplete in 40 ns simulations (data not shown). Consequently, initial conditions for the simulations reported here were developed with fully formed and well-equilibrated (40 ns) spherical micelles in ~5500 waters.

Experimental evidence indicates that the peptide is disordered in solution and largely α-helical in the micelle. To explore potential force field (FF) dependencies, 50 ns simulations of the peptide in water and in an α-helix were carried out with CHARMM22/CMAP (30,31), GROMOS96 (53a6) (32), and OPLS-AA (33). The α-helix remained stable over the entire trajectory with CHARMM22/CMAP, rapidly converted to a stable π-helix with GROMOS96, and became disordered within 13 ns with OPLA-AA. Based on these results, the OPLS-AA FF was chosen for peptide, DPC, and SDS (with one change noted below).

All simulations and analyses were performed using the GROMACS 3.3.1 simulation package (34,35). Coordinates of the SDS molecule were generated using the PRODRG2 server (36). The united-parameter set for lipids was downloaded from http://moose.bio.ucalgary.ca, and charges of SDS headgroup were set equal to those in the CHARMM FF (37) (these charges

were not available in OPLS). All-atom OPLS parameters (33) were used for the peptide. Five initial conditions were constructed (Table 1 and see Fig. 6). *SDS1*, *SDS2*, and *SDS3* contained 75 lipids (the experimentally established aggregation number for SDS micelles) (38). *SDS4* contained 40 lipids to investigate effects of micelle size, and *DPC* contained 65 monomers of DPC. Initial coordinates for the N-BAR peptide were those of the lowest energy structure from the NMR ensemble, which is 76% α-helical. The peptides were placed in different orientations and positions with respect to the micelle as specified in Table 1. A hole for the inserting peptide was made by following the hole protocol (39). The MSMS program was used for scanning the surface of peptides (40), and then a hole-making force was introduced to the scanned surface of the peptide. The peptide was inserted into the resulting hole, and then energy minimization was performed with position restraints applied to the peptide. Approximately 16,000 TIP4P water molecules (41) were placed around a mixture of the peptide and micelle to a thickness of 1 nm, forming a periodic box sized $8 \times 8 \times 8$ nm^3. Na^+ ions were added to neutralize charges from the SDS molecules. For DPC, the equilibrated 65-surfactant DPC micelle was downloaded from http://moose.bio.ucalgary.ca, and the same procedures were performed with 5 Cl^- ions added to neutralize the peptide. A cutoff of 1.1 nm was set for the van der Waals interactions with particle mesh Ewald summation used for electrostatic interactions (42). A pressure of 1 bar and a temperature of 298 K were maintained in an NPT ensemble by applying the Berendsen coupling method with the time constants of 0.1 and 1.0 ps for temperature and pressure, respectively (43). After energy minimization with 200 steps of steepest descent, unrestrained trajectories were carried out for 60 ns with a time step of 2 fs. Coordinates were saved every picosecond, and averages were obtained from the last 20 ns. The secondary structure of the peptide was calculated using the DSSP program (44).

Protein structure accession number

The coordinates of the structure of the N-BAR peptide in DPC and SDS micelles have been deposited in the Protein Data Bank under the accession numbers 2RND and 2RMY.

RESULTS AND DISCUSSION

The predicted N-terminal amphipathic helix-0 of the human Bin1/Amphiphysin II BAR domain comprises residues 1–33 (14,45). This part of the molecule is disordered in the absence of lipids and thereby unresolved in the crystal structure (12). The N-BAR peptide studied here (^{1}MAEMGSKGV^{10}TAGKIASNVQ^{20}KKLTRAQEKV^{30}LQKLY) contains an additional tyrosine residue at the C-terminus of helix-0 for spectroscopic reasons. DPC and SDS micelles were chosen because they have been successfully used for other peptide and protein structure determinations by NMR spectroscopy (46–49).

TABLE 1 Composition and initial conditions for the N-BAR peptide/micelle simulations

	Micelles		Initial position of the peptide	
Name	Type	No. lipids	Location	Orientation of hydrophobic residues
SDS1	SDS	75	Water region	Toward micelle
SDS2	SDS	75	Water region	Away from micelle
SDS3	SDS	75	Inside micelle	–
SDS4	SDS	40	Inside micelle	–
DPC	DPC	65	Inside micelle	–

Structure induction upon membrane binding

Far-UV CD spectra of the full-length N-BAR domain revealed an increased helicity after adding brain lipid liposomes (Fig. 1 *a*, *solid lines*). The helical content of a deletion mutant lacking the first 31 residues (BAR) did not change in the presence of lipids. The isolated N-BAR peptide is unstructured in aqueous solution (Fig. 1 *b*, *solid black line*). As in the full-length protein, the ellipticity minima at 208 and 222 nm indicate that the peptide takes on a helical structure when bound to liposomes or micelles. The CD spectra of the N-BAR peptide in brain lipid liposomes or DPC or SDS micelles are virtually identical, indicating a similar secondary structure under these conditions (Fig. 1 *b*). In 60% tetrafluoroethylene, the helical content increased further, indicating that not all residues of the N-BAR peptide are in a helical conformation in the presence of detergents or lipids. A helical wheel projection (see Fig. 3*d*) of the peptide highlights its amphipathic character (that is, hydrophobic and charged/polar residues are located opposite to each other). Conspicuous is the high number of lysine residues, implying that binding and structure induction of the N-BAR peptide is driven by hydrophobic and electrostatic interactions. This finding is further supported by the observation that nonionic OG micelles as membrane mimetics do not lead to structuring of the peptide as observed by the far-UV CD spectrum (Fig. 1 *b*, *dashed light gray*).

NMR structure and dynamics of N-BAR peptide

Binding of the N-BAR peptide to micelles results in a deviation of the backbone and, more obviously, the side-chain resonances in the ^{15}N-HSQC spectrum (Fig. 2 *b*) from the random coil chemical shifts dominating the spectrum in

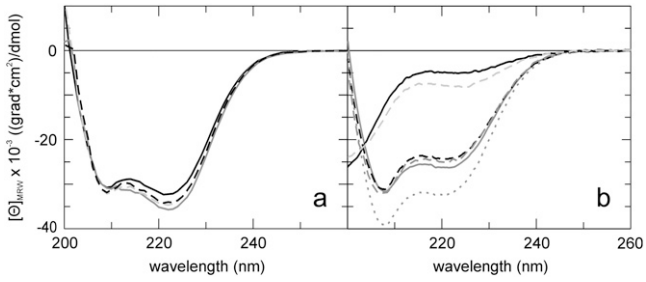

FIGURE 1 Far-UV CD spectra of the BAR domain and the N-terminal N-BAR peptide in various solvent environments. (*a*) CD spectra of the N-BAR (residues 1–241) (*solid line*) and the BAR (residues 32–241) domain (*dashed line*) of human amphiphysin II in the presence and absence of brain lipid liposomes (*gray* and *black, respectively*). Structure induction on binding to liposomes is only seen for the N-BAR domain (*solid gray line*), indicated by a significant signal decrease at 222 nm. (*b*) The N-BAR peptide is unstructured in solution (*solid black line*). In the presence of liposomes (*dashed dark gray line*), SDS (*solid gray line*) or DPC (*black dashed line*) micelles, the peptide becomes structured. In the presence of OG (*dashed light gray line*) micelles, however, no structure induction is observed. A CD spectrum recorded in 60% trifluoroethanol (*dotted line*) shows the greatest helical content.

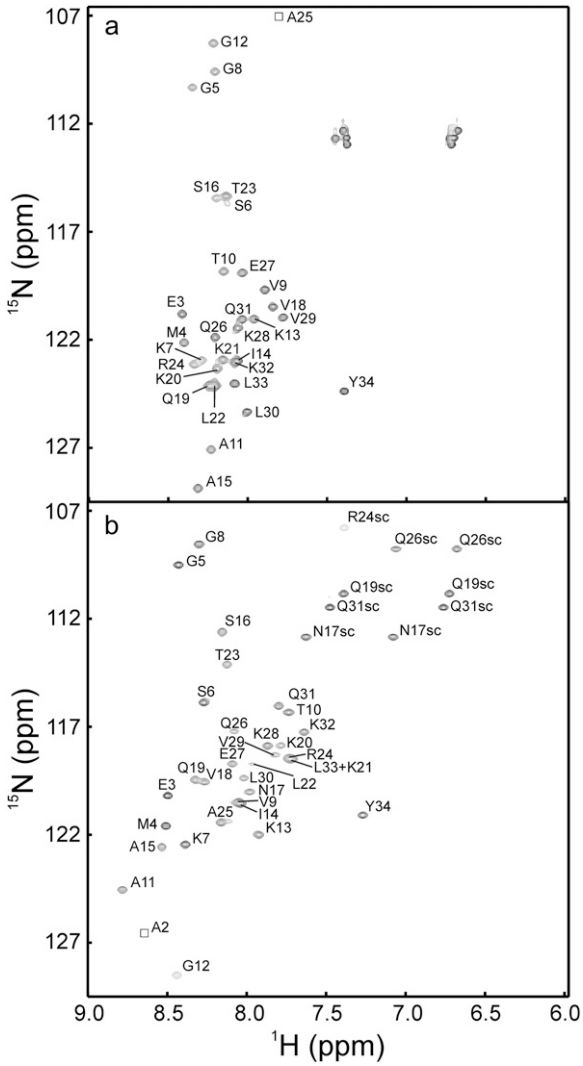

FIGURE 2 2D ^{1}H-^{15}N HSQC spectra of the N-BAR peptide (*a*) in aqueous solution and (*b*) bound to DPC micelles. The assigned crosspeaks of the backbone amides are labeled using the one-letter amino acid code and the sequence position. Boxes indicate resonance signals, which show crosspeak intensities below the plotted contour level. The respective spectrum of N-BAR peptide in SDS micelles is shown in Fig. S11 in Data S1.

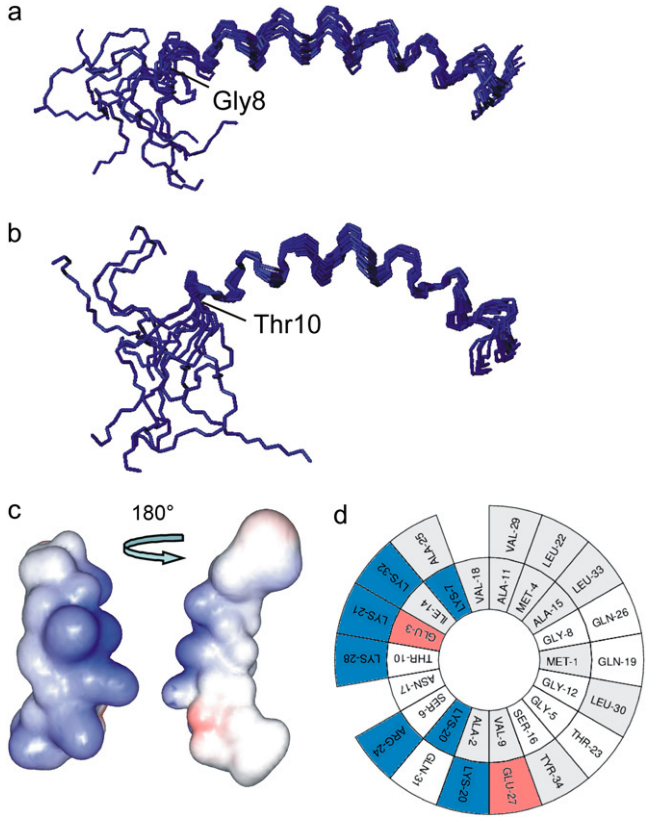

FIGURE 3 Structure ensembles of the N-BAR peptide backbone bound to detergent micelles at 25°C: 10 lowest energy structures in (*a*) SDS micelles and (*b*) DPC micelles. (*c*) Electrostatic surface potential representation of the N-BAR peptide in DPC micelles. Negative potentials are shown in red and positive potentials in blue. (*d*) Helical wheel diagram for the N-BAR peptide. The amino acid sequence is plotted clockwise. Hydrophobic residues are shown in gray boxes, and positively and negatively charged residues are shown in blue and red boxes, respectively.

aqueous solution (Fig. 2 *a*). This finding confirms the interaction of N-BAR with the micellar environment and the induction of a defined secondary structure in SDS or DPC observed by far-UV CD spectra. All backbone and side-chain resonances were assigned as described in Materials and Methods. More than 500 NOE distance constraints were derived from two-dimensional NOESY and ^{15}N-NOESY-HSQC spectra in the presence of either SDS or DPC micelles. By using all experimentally determined constraints (NOEs, dihedral angles derived from J couplings, and chemical shifts), ensembles of structures of the N-BAR peptide in SDS (Fig. 3 *a*) and DPC (Fig. 3 *b*) micelles were calculated; structural statistics are provided in Table S2 in Data S1. Residues 8–34 in SDS and 10–34 in DPC micelles are well-ordered with a heavy atom root mean-square deviation < 1.1 Å. This α-helical content is consistent with the CD data (Fig. 1). Hence, the structured part of the N-BAR peptide is an amphipathic helix with the negatively charged side chains on the convex side and the hydrophobic side chains on the concave side (Fig. 3 *c*).

The disordering of the N-terminus results from fast and large-amplitude local dynamics confirmed by ^{15}N-heteronuclear NOE (hNOE) measurements (Fig. 4). hNOE values > 0.5 are typical for structural elements in peptides and proteins that are relatively rigid on a timescale of nanoseconds to picoseconds. For the N-BAR peptide in SDS and DPC micelles, the hNOE gradually decreases from T10 toward the N-terminus and is even negative for the first residues. Therefore, the dynamic data agree well with the loss of NOE constraints in the highly flexible and disordered conformation at the N-terminus. In comparison, all hNOE values of the N-BAR peptide in aqueous solution (Fig. 4 *c*) are close to zero or negative. Taken together with a lack of medium-range NOEs over the entire sequence, a random coil conformation in the absence of detergent and lipids can be concluded. The hNOE of an extended

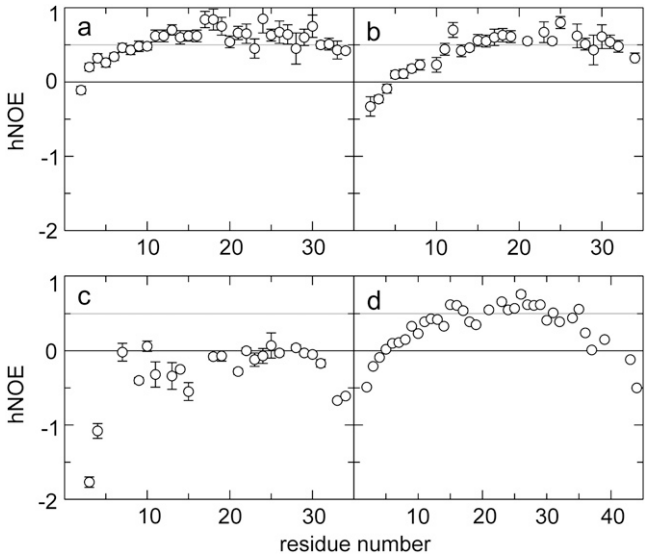

FIGURE 4 ^{1}H-^{15}N heteronuclear NOEs of the N-BAR peptide in (*a*) SDS, (*b*) DPC, and (*c*) aqueous solution. (*d*) hNOE values of the extended N-BAR peptide (1–44 residues).

N-BAR peptide in DPC micelles with 44 amino acids drops after K35 toward the C-terminus, indicating that the amphipathic helix ends at position 35 and following residues form the linker to helix-1 of the BAR domain.

Fast (millisecond) amide proton exchange

To determine which regions of the N-BAR peptide were buried in the detergent micelle, fast (millisecond) amide proton exchange was measured for each residue by NMR (24); examples of exchange curves are depicted in Fig. 5. This approach is straightforward compared to the use of spin labels (50), because the NMR sample for structure determination can be used without further modifications. N-terminal, polar, and charged residues showed a pronounced signal change during the experiment (Fig. 5, *red*), indicating fast-exchanging amide protons because of an increased solvent accessibility and a dynamic open and closing of the corresponding hydrogen bonds on the millisecond-second timescale. Amide protons of hydrophobic residues, however, did not exchange at all (Fig. 5, *blue*), because they are buried in the micelle and therefore shielded from the solvent. Furthermore, residues 1–11, the region with high, local fluctuations derived from dynamic data (Fig. 4, *b* and *c*), showed low protection against exchange of the amide protons.

MD simulation of the N-BAR peptide

As an independent complement to the preceding experimental results, MD simulations were carried out on the N-BAR peptide in micelles with different surfactants, micelle sizes, and initial configurations to investigate helical stability,

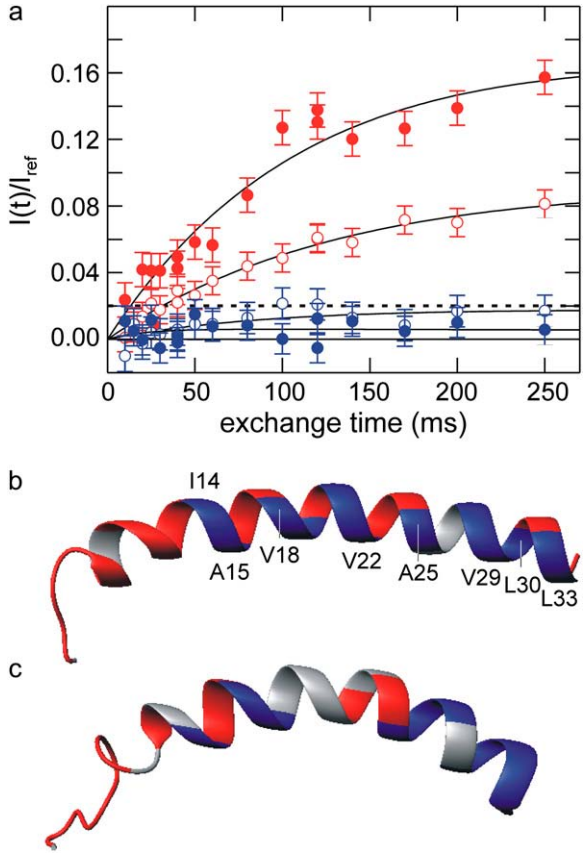

FIGURE 5 NMR experiment to detect fast-exchanging amide protons (MEXICO) of the N-BAR peptide bound to SDS and DPC micelles. Fast amide proton exchange was followed on a residue by residue level. (*a*) Exchange curves in SDS micelles are shown for T23 (*solid red symbols*), S16 (*open red symbols*), L33 (*solid blue symbols*), and V29 (*open blue symbols*). Fast-exchanging amides are colored in red. Amide protons, which did not exchange within the timescale of the experiment (*below dashed line*; see Fig. S12 in Data S1) are colored in blue. Exchange curves for residues in gray could not been evaluated due to signal overlap or low signal intensity. This color code was assigned to a ribbon representation of the lowest energy NMR structure of the N-BAR peptide in (*b*) SDS and (*c*) DPC micelles.

peptide orientation, and depth of insertion in the micelle environment. Fig. 6 shows snapshots at the beginning (*left*) and end (*right*) of the five 60 ns simulations of peptide/micelle complex simulations (Table 1). In each case, the peptide migrated to the surface of the micelle. The micelle remained spherical, and the peptide curved. In pure water, the N-BAR peptide partially unfolds in the first nanosecond and loses almost all helicity by 13 ns (see Fig. S9 in Data S1). Hence, the micelle environment generally stabilizes the helix, leading to a range of α-helicities of 40 to 50% (SDS1: 48%; SDS3: 50%; DPC: 40%) for residues 12–30 during the final simulated 20 ns. The helical instability of the N-terminal residues agrees with the amide proton exchange and the NMR relaxation data (Figs. 4 and 5). The SDS4 simulation (the smaller micelle) yielded a slightly lower helical content (30%). It is possible that the higher curvature imposed on the peptide for binding led to this instability. As evident in Fig. 6, the N-BAR peptide

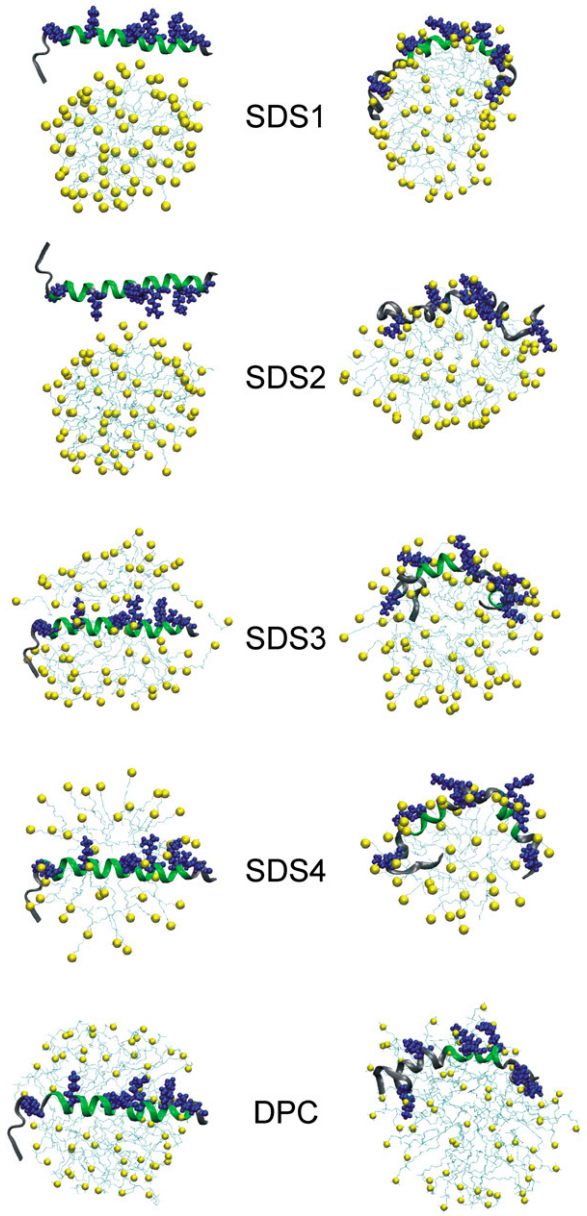

FIGURE 6 Snapshots at the beginning (*left*) and end (*right*) of 60 ns simulations of the peptide/micelle systems denoted SDS1, SDS2, SDS3, SDS4, and DPC (Table 1). α-Helical regions of the peptides are presented in green, nonhelical in gray, and positively charged side chains in blue. The negatively charged sulfur of SDS and phosphorous of DPC are yellow, and the acyl chains are light blue. The N-BAR peptide is initially positioned inside or outside a micelle. Water and ions are omitted for clarity. The images were created using visual MD (52).

bound to the micelle with little (6%) α-helicity in the SDS2 trajectory. This observation can be attributed to the initial condition in which the cationic residues of the peptide were oriented toward the micelle. When the peptide interacts with the micelle, cationic and hydrophobic residues, respectively, have favorable interactions with SDS headgroups and tails, which may lead to a flip of the peptide and instability of the helical structure. It is possible that the peptide in SDS2 would refold to the helical form in much longer simulations, but this observation is outside the scope of this study. Our results indicate that MD simulations can represent the experimentally measured stability of the peptide, although the final configuration is partially determined by initial configuration and micelle size. Further analyses are based on SDS1, SDS3, and DPC.

Orientation of the peptide in micelles

Experimental results from fast proton exchange experiments of backbone amides are compared in Fig. 7 *a* with the solvent accessible surface area (SASA) calculated for SDS3. Between A11 and Y34, the SASA correlates well with the hydrophobic residues (Fig. 7 *a*, *squares*) and residues with low exchange rates (Fig. 7 *a*, *black symbols*) buried in the micelle, whereas charged residues face toward water. This correlation is less pronounced for the DPC micelle (see Fig. S10 in Data S1). To investigate factors controlling the depth of penetration of the N-BAR peptide, radial distribution functions (g(r)) between

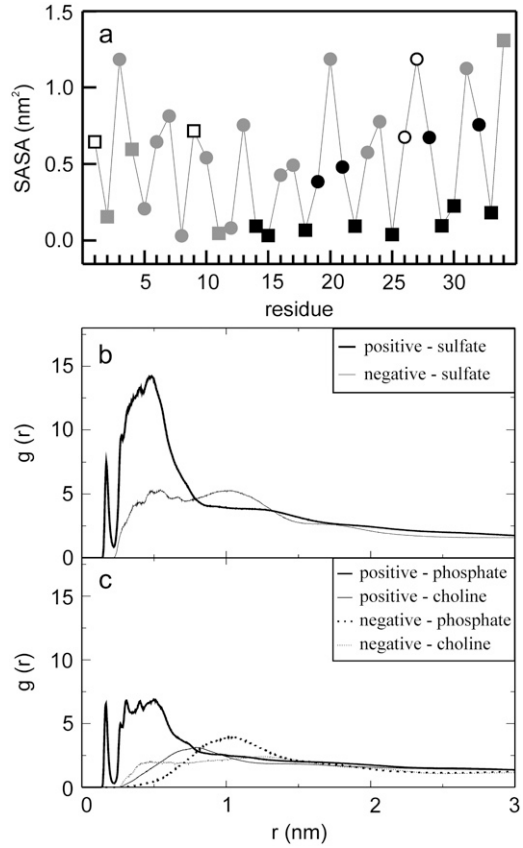

FIGURE 7 (*a*) Solvent accessible surface areas per residue of the N-BAR peptide in SDS micelles (SDS3 simulation). Squares represent hydrophobic residues shown in Fig. 3 *d*. Black symbols correspond to residues not exposed to water according to the amide proton exchange experiments. Gray denotes fast-exchanging protons, and white represents missing experimental data. Radial distribution functions g(r) for charged residues of the peptide with respect to SDS headgroups in SDS3 (*b*) and DPC headgroups in DPC (*c*) averaged over the last 20 ns.

charged residues of the peptide and lipid headgroups were calculated for SDS3 and DPC. The integral of g(r) over a particular interval is proportional to the coordination number in that interval. Fig. 7, *b* and *c*, shows that g(r) of the lipid headgroups around cationic residues of the peptide is substantially higher than for anionic residues. Moreover, in the DPC micelles, g(r) of the phosphate headgroups around cationic residues of the peptide have higher values compared to the choline headgroups around both anionic and cationic residues of the peptide. These results imply that cationic residues of the peptide strongly interact with anionic lipid headgroups and that the N-BAR peptide embeds deeper in the DPC micelle compared to SDS.

Tubulation of liposomes

The ability of BAR domains to generate membrane curvature has been shown in vitro (13,17,20,21,51) by the formation of narrow tubes of liposomes. To investigate the significance of helix-0 in this process, we determined changes in the shape of liposomes in the presence of different BAR domain constructs by EM. The human amphiphysin N-BAR domain can constrict liposomes into tubules but leads to vesiculation at higher protein concentrations (Fig. 8 *b*) (13). A deletion mutant lacking the N-terminal amphipathic helix (BAR) had much less influence on the liposome morphology (Fig. 8 *c*). In addition to extensive vesiculation, tube formation was observed for the N-BAR peptide (Fig. 8, *d* and *e*) and the extended 1–44 residue N-BAR peptide (Fig. 8 *f*). FRET-based membrane fusion assays yield a more quantitative measure of the membrane fusion properties of the different BAR domain constructs. Liposomes were prepared with fluorescence-labeled lipids and subsequently mixed with unlabeled liposomes; fusion of labeled with unlabeled liposomes can be followed by the quench of the FRET signal concomitant with an increase of the donor fluorescence at 530 nm. Fig. 8, *g* and *h*, shows membrane fusion for the N-BAR domain and the N-BAR peptides but not for the BAR domain lacking helix-0.

CONCLUSIONS

This study combines experimental and theoretical techniques to obtain detailed insights into the structural properties of helix-0 of human Bin1/Amphiphysin II BAR domain. Because structural information for the interaction of proteins and lipids requires the introduction of mutations and spin labels (20), the N-BAR peptide was investigated when bound to detergent micelles and during tubulation of liposomes. Experiment and simulation confirmed the predicted transition from random coil to helix upon micelle binding but revealed an unstructured and solvent-exposed N-terminal region. Binding and amphipathic structure induction is mediated by hydrophobic and electrostatic interactions. The MD simulations completed the structural view of the N-BAR peptide in the SDS and DPC micelles that were derived from the NMR structure calculations in vacuum. The robustness of the sim-

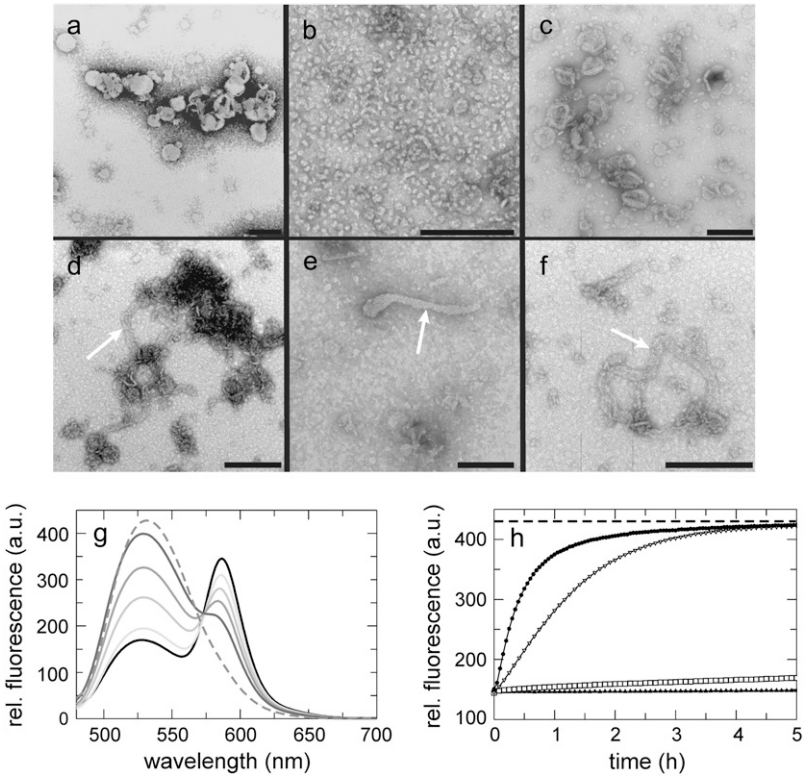

FIGURE 8 Electron micrographs of liposome tubulation by (*b*) human amphiphysin N-BAR, (*c*) BAR, and (*d* and *e*) the N-BAR peptide (length scale: black bar, 200 nm). Untreated liposomes are shown in *a* and in the presence of an extended N-BAR peptide (residues 1–44) in *f*. Emission spectra (*g*) from mixed liposomes in the absence (*black curve*) and presence of the N-BAR domain at various time points (8 min, 28 min, 62 min, 225 min; *light* to *dark gray*) and 1% Triton (for total donor fluorescence; *dashed line*). (*h*) Time-dependent increase of donor fluorescence at 530 nm upon membrane fusion in the presence of N-BAR (*solid circles*), BAR (*open squares*) and the N-BAR peptide (*open triangles*). Fluorescence change caused by spontaneous liposome fusion is negligible (*solid squares*) and at maximum in 1% Triton (*dashed line*).

ulations is reflected by comparable final conformations of the N-BAR peptide starting from different conditions and by the peptide curvature, which was maintained during the simulation and adapts to the micelle. A slightly increased curvature of the N-BAR peptide in DPC micelles compared to SDS found in the calculated NMR structures (Fig. 3, *a* and *b*) is a result of several side-chain-side-chain and backbone-side-chain NOEs, which were unambiguously identified. This curvature might result from the more deeply embedded peptide caused by the polar interactions with the zwitterionic DPC headgroups, if we assume the same spherical size of both micelle types.

Recent experiments based on fluorescence measurements imply an antiparallel dimer formation of the helix-0 of the BRAP/Bin2 BAR domain (breast cancer-associated protein) when bound to liposomes (14). In this study, no long-range NOEs between N- and C-terminal residues of the N-BAR peptide were observed in the NOESY spectra, which rules out dimer formation. Nevertheless, oligomerization of the helix-0 under different conditions cannot be excluded because the structure was determined in detergent micelles with a high detergent/peptide ratio.

Recently, a point mutation (K35N) in the helix-0 of the human Bin1/Amphiphysin II N-BAR domain found in patients suffering from autosomal recessive centronuclear myopathy reduced the number and length of tubules in ex vivo membrane assays (11). In isolation at least, extended N-BAR peptides comprising 1–44 residues with K35 and N35 could not be distinguished from the 1–34 peptide in the biophysical measurements (CD and NMR spectra, tubulation) presented here. The tubulation experiments, however, did reveal the importance of helix-0 for changing membrane morphology of liposomes by itself or when present in the BAR domain.

In summary, this work highlights the importance of the amphipathic helix-0 for increasing the affinity of the N-BAR domain to lipid bilayers. It also helps differentiate current models of curvature generation by the N-BAR domain. Although these findings do not definitively rule out the spontaneous curvature and bilayer-coupling mechanics, they favor the scaffold mechanism. Therefore, we expect little curvature generation preceding the main interaction with the entire N-BAR domain.

SUPPLEMENTARY MATERIAL

To view all of the supplemental files associated with this article, visit www.biophysj.org.

We thank Paul Rösch for NMR spectrometer time at 600, 700, and 800 MHz; Gerd Hause and Rolf Sachs for electron microscopy; Andreas Kerth for help with liposome preparation; and Alfred Blume for helpful discussions.

This research was supported in part by a grant from the Deutsche Forschungsgemeinschaft (Ba 1821/3-1 and GRK 1026); the Excellence Initiative of the State Sachsen-Anhalt; the Intramural Research Program of the National Institutes of Health (NIH), National Heart, Lung and Blood Institute; and the CIT Biowulf/LoBoS3 cluster at the NIH for use of the high-performance computational capabilities.

REFERENCES

1. David, C., P. S. McPherson, O. Mundigl, and P. de Camilli. 1996. A role of amphiphysin in synaptic vesicle endocytosis suggested by its binding to dynamin in nerve terminals. *Proc. Natl. Acad. Sci. USA.* 93:331–335.
2. Shupliakov, O., P. Low, D. Grabs, H. Gad, H. Chen, C. David, K. Takei, P. De Camilli, and L. Brodin. 1997. Synaptic vesicle endocytosis impaired by disruption of dynamin-SH3 domain interactions. *Science.* 276:259–263.
3. Ren, G., P. Vajjhala, J. S. Lee, B. Winsor, and A. L. Munn. 2006. The BAR domain proteins: molding membranes in fission, fusion, and phagy. *Microbiol. Mol. Biol. Rev.* 70:37–120.
4. Di Paolo, G., S. Sankaranarayanan, M. R. Wenk, L. Daniell, E. Perucco, B. J. Caldarone, R. Flavell, M. R. Picciotto, T. A. Ryan, O. Cremona, and P. De Camilli. 2002. Decreased synaptic vesicle recycling efficiency and cognitive deficits in amphiphysin 1 knockout mice. *Neuron.* 33:789–804.
5. Zhang, B., and A. C. Zelhof. 2002. Amphiphysins: raising the BAR for synaptic vesicle recycling and membrane dynamics. Bin-Amphiphysin-Rvsp. *Traffic.* 3:452–460.
6. Lee, E., M. Marcucci, L. Daniell, M. Pypaert, O. A. Weisz, G. C. Ochoa, K. Farsad, M. R. Wenk, and P. De Camilli. 2002. Amphiphysin 2 (Bin1) and T-tubule biogenesis in muscle. *Science.* 297:1193–1196.
7. McMahon, H. T., and J. L. Gallop. 2005. Membrane curvature and mechanisms of dynamic cell membrane remodelling. *Nature.* 438:590–596.
8. Dawson, J. C., J. A. Legg, and L. M. Machesky. 2006. Bar domain proteins: a role in tubulation, scission and actin assembly in clathrin-mediated endocytosis. *Trends Cell Biol.* 16:493–498.
9. Shimada, A., H. Niwa, K. Tsujita, S. Suetsugu, K. Nitta, K. Hanawa-Suetsugu, R. Akasaka, Y. Nishino, M. Toyama, L. Chen, Z. J. Liu, B. C. Wang, M. Yamamoto, T. Terada, A. Miyazawa, A. Tanaka, S. Sugano, M. Shirouzu, K. Nagayama, T. Takenawa, and S. Yokoyama. 2007. Curved EFC/F-BAR-domain dimers are joined end to end into a filament for membrane invagination in endocytosis. *Cell.* 129:761–772.
10. Henne, W. M., H. M. Kent, M. G. Ford, B. G. Hegde, O. Daumke, P. J. Butler, R. Mittal, R. Langen, P. R. Evans, and H. T. McMahon. 2007. Structure and analysis of FCHo2 F-BAR domain: a dimerizing and membrane recruitment module that effects membrane curvature. *Structure.* 15:839–852.
11. Nicot, A. S., A. Toussaint, V. Tosch, C. Kretz, C. Wallgren-Pettersson, E. Iwarsson, H. Kingston, J. M. Garnier, V. Biancalana, A. Oldfors, J. L. Mandel, and J. Laporte. 2007. Mutations in amphiphysin 2 (BIN1) disrupt interaction with dynamin 2 and cause autosomal recessive centronuclear myopathy. *Nat. Genet.* 39:1134–1139.
12. Casal, E., L. Federici, W. Zhang, J. Fernandez-Recio, E. M. Priego, R. N. Miguel, J. B. DuHadaway, G. C. Prendergast, B. F. Luisi, and E. D. Laue. 2006. The crystal structure of the BAR domain from human Bin1/amphiphysin II and its implications for molecular recognition. *Biochemistry.* 45:12917–12928.
13. Peter, B. J., H. M. Kent, I. G. Mills, Y. Vallis, P. J. Butler, P. R. Evans, and H. T. McMahon. 2004. BAR domains as sensors of membrane curvature: the amphiphysin BAR structure. *Science.* 303:495–499.
14. Fernandes, F. M., L. M. Loura, F. J. Chichon, J. L. Carrascosa, A. Fedorov, and M. Prieto. 2008. Role of Helix-0 of the N-BAR domain in membrane curvature generation. *Biophys. J.* 94:3065–3073.
15. Takei, K., V. I. Slepnev, V. Haucke, and P. De Camilli. 1999. Functional partnership between amphiphysin and dynamin in clathrin-mediated endocytosis. *Nat. Cell Biol.* 1:33–39.
16. Blood, P. D., and G. A. Voth. 2006. Direct observation of Bin/amphiphysin/Rvs (BAR) domain-induced membrane curvature by means of molecular dynamics simulations. *Proc. Natl. Acad. Sci. USA.* 103:15068–15072.
17. Farsad, K., N. Ringstad, K. Takei, S. R. Floyd, K. Rose, and P. De Camilli. 2001. Generation of high curvature membranes mediated by direct endophilin bilayer interactions. *J. Cell Biol.* 155:193–200.

18. Ford, M. G., I. G. Mills, B. J. Peter, Y. Vallis, G. J. Praefcke, P. R. Evans, and H. T. McMahon. 2002. Curvature of clathrin-coated pits driven by epsin. *Nature*. 419:361–366.

19. Lee, M. C., L. Orci, S. Hamamoto, E. Futai, M. Ravazzola, and R. Schekman. 2005. Sar1p N-terminal helix initiates membrane curvature and completes the fission of a COPII vesicle. *Cell*. 122:605–617.

20. Gallop, J. L., C. C. Jao, H. M. Kent, P. J. Butler, P. R. Evans, R. Langen, and H. T. McMahon. 2006. Mechanism of endophilin N-BAR domain-mediated membrane curvature. *EMBO J*. 25:2898–2910.

21. Masuda, M., S. Takeda, M. Sone, T. Ohki, H. Mori, Y. Kamioka, and N. Mochizuki. 2006. Endophilin BAR domain drives membrane curvature by two newly identified structure-based mechanisms. *EMBO J*. 25:2889–2897.

22. Zimmerberg, J., and M. M. Kozlov. 2006. How proteins produce cellular membrane curvature. *Nat. Rev. Mol. Cell Biol.* 7:9–19.

23. Bosse-Doenecke, E., U. Weininger, M. Gopalswamy, J. Balbach, S. Möller Knudsen, and R. Rudolph. 2008. High yield production of recombinant native and modified peptides exemplified by ligands for G-protein coupled receptors. *Protein Expr. Purif.* 58:114–121.

24. Koide, S., W. Jahnke, and P. E. Wright. 1995. Measurement of intrinsic exchange rates of amide protons in a 15N-labeled peptide. *J. Biomol. NMR*. 6:306–312.

25. Delaglio, F., S. Grzesiek, G. W. Vuister, G. Zhu, J. Pfeifer, and A. Bax. 1995. NMRPipe: a multidimensional spectral processing system based on UNIX pipes. *J. Biomol. NMR*. 6:277–293.

26. Johnson, B. A. 2004. Using NMRView to visualize and analyze the NMR spectra of macromolecules. *Methods Mol. Biol.* 278:313–352.

27. Linge, J. P., M. Habeck, W. Rieping, and M. Nilges. 2003. ARIA: automated NOE assignment and NMR structure calculation. *Bioinformatics*. 19:315–316.

28. Cornilescu, G., F. Delaglio, and A. Bax. 1999. Protein backbone angle restraints from searching a database for chemical shift and sequence homology. *J. Biomol. NMR*. 13:289–302.

29. Laskowski, R. A., J. A. Rullmannn, M. W. MacArthur, R. Kaptein, and J. M. Thornton. 1996. AQUA and PROCHECK-NMR: programs for checking the quality of protein structures solved by NMR. *J. Biomol. NMR*. 8:477–486.

30. MacKerell, A. D., Jr., M. Feig, and C. L. Brooks 3rd. 2004. Extending the treatment of backbone energetics in protein force fields: limitations of gas-phase quantum mechanics in reproducing protein conformational distributions in molecular dynamics simulations. *J. Comput. Chem.* 25:1400–1415.

31. Brooks, B. R., R. E. Bruccoleri, B. D. Olafson, D. J. States, S. Swaminathan, and M. J. Karplus. 1983. CHARMM: a program for macromolecular energy, minimization, and dynamics calculations. *J. Comp. Chem.* 4:187–217.

32. Oostenbrink, C., A. Villa, A. E. Mark, and W. F. van Gunsteren. 2004. A biomolecular force field based on the free enthalpy of hydration and solvation: the GROMOS force-field parameter sets 53A5 and 53A6. *J. Comput. Chem.* 25:1656–1676.

33. Jorgensen, W. L., and J. Tirado-Rives. 1988. The OPLS potential functions for proteins. Energy minimization for crystals of cyclic peptides and crambin. *J. Am. Chem. Soc.* 110:1657–1666.

34. Lindahl, E., B. Hess, and D. van der Spoel. 2001. GROMACS 3.0: a package for molecular simulation and trajectory analysis. *J. Mol. Mod.* 7:306–317.

35. van der Spoel, D., E. Lindahl, B. Hess, G. Groenhof, A. E. Mark, and H. J. Berendsen. 2005. GROMACS: fast, flexible, and free. *J. Comput. Chem.* 26:1701–1718.

36. Schüttelkopf, A. W., and D. M. van Aalten. 2004. PRODRG: a tool for high-throughput crystallography of protein-ligand complexes. *Acta Crystallogr. D Biol. Crystallogr.* 60:1355–1363.

37. MacKerell, A. D., Jr. 1995. Molecular dynamics simulation analysis of a sodium dodecyl sulfate micelle in aqueous solution: decreased fluidity of the micelle hydrocarbon interior. *J. Phys. Chem.* 99:1846–1855.

38. Bales, B. L., and M. Almgren. 1995. Fluorescence quenching of pyrene by copper (II) in sodium dodecyl sulfate micelles. Effect of micelle size as controlled by surfactant concentration. *J. Phys. Chem.* 99:15153–15162.

39. Faraldo-Gomez, J. D., G. R. Smith, and M. S. Sansom. 2002. Setting up and optimization of membrane protein simulations. *Eur. Biophys. J.* 31:217–227.

40. Sanner, M. F., A. J. Olson, and J. C. Spehner. 1996. Reduced surface: an efficient way to compute molecular surfaces. *Biopolymers*. 38:305–320.

41. Jorgensen, W. L., J. Chandrasekhar, J. D. Madura, R. W. Impey, and M. L. Klein. 1983. Comparison of simple potential functions for simulating liquid water. *J. Chem. Phys.* 79:926–935.

42. Essmann, U., L. Perera, M. L. Berkowitz, T. Darden, H. Lee, and L. G. Pedersen. 1995. A smooth particle mesh Ewald method. *J. Chem. Phys.* 103:8577–8593.

43. Berendsen, H. J. C., J. P. M. Postma, W. F. van Gunsteren, A. Dinola, and J. R. Haak. 1984. Molecular dynamics with coupling to an external bath. *J. Chem. Phys.* 81:3684–3690.

44. Kabsch, W., and C. Sander. 1983. Dictionary of protein secondary structure: pattern recognition of hydrogen-bonded and geometrical features. *Biopolymers*. 22:2577–2637.

45. Gallop, J. L., and H. T. McMahon. 2005. BAR domains and membrane curvature: bringing your curves to the BAR. *Biochem. Soc. Symp.* 223–231.

46. Han, X., J. H. Bushweller, D. S. Cafiso, and L. K. Tamm. 2001. Membrane structure and fusion-triggering conformational change of the fusion domain from influenza hemagglutinin. *Nat. Struct. Biol.* 8:715–720.

47. Liang, B., and L. K. Tamm. 2007. Structure of outer membrane protein G by solution NMR spectroscopy. *Proc. Natl. Acad. Sci. USA*. 104:16140–16145.

48. Kessler, H., D. F. Mierke, J. Saulitis, S. Seip, S. Steuernagel, T. Wein, and M. Will. 1992. The structure of Ro 09–0198 in different environments. *Biopolymers*. 32:427–433.

49. Koppitz, M., B. Mathä, and H. Kessler. 1999. Structure investigation of amphiphilic cyclopeptides in isotropic and anisotropic environments-A model study simulating peptide-membrane interactions. *J. Pept. Sci.* 5:507–518.

50. Neumoin, A., B. Arshava, J. Becker, O. Zerbe, and F. Naider. 2007. NMR studies in dodecylphosphocholine of a fragment containing the seventh transmembrane helix of a G-protein-coupled receptor from Saccharomyces cerevisiae. *Biophys. J.* 93:467–482.

51. Richnau, N., A. Fransson, K. Farsad, and P. Aspenstrom. 2004. RICH-1 has a BIN/Amphiphysin/Rvsp domain responsible for binding to membrane lipids and tubulation of liposomes. *Biochem. Biophys. Res. Commun.* 320:1034–1042.

52. Humphrey, W., A. Dalke, and K. Schulten. 1996. VMD: visual molecular dynamics. *J. Mol. Graph.* 14:33–38.